Journal of Fluorescence, Vol. 1, No. 1, 1991

Continuous Lifetime Distributions of β-Cyclodextrin–Anilinonaphthalene Sulfonic Acid Inclusion Complexes

Gino C. Catena[1] and Frank V. Bright[1,2]

Received October 18, 1990; revised December 7, 1990; accepted December 7, 1990

Fluorescence lifetimes are reported for a series of anilinonaphthalene sulfonate (ANS) probe molecules complexed with β-cyclodextrin (β-CD). The fluorescence decay kinetics are recovered by multifrequency phase and modulation measurements in concert with a global analysis scheme. In all cases studied, a continuous Lorentzian distribution of lifetimes is observed, resulting from the dynamical nature of the ANS–β-CD complex and free ANS. Trends are discussed and comparisons made between bound and free fluorophore and between different isomeric ANS structures.

KEY WORDS: Distribution analysis; multifrequency phase-modulation fluorescence; cyclodextrins; inclusion complexes.

INTRODUCTION

Cyclodextrins (CDs) are torroidally shaped polysaccharides made up of six to eight ($\alpha = 6$, $\beta = 7$, $\gamma = 8$) D-glucose monomers linked covalently at the 1 and 4 carbon atoms. The internal cavities are relatively hydrophobic and have diameters ranging from 4.7 to 8.3 Å [1,2]. Because of their unique structure, CDs can sequester (i.e., host or include) a variety of small molecules or small molecular moieties within their cavity. In these complexes, noncovalent, intermolecular forces play the primary role in complex formation and stabilization [1,2]. Accordingly, these complexes are useful in synthetic methods as enzyme mimics [3] and as models for protein–substrate binding [4].

CDs have also been used extensively in numerous analytical applications. For example, Armstrong and coworkers have employed immobilized cyclodextrins as stationary phases in high-performance liquid chromatography (HPLC) [5] and gas chromatography (GC) [6]. In addition, Cline-Love's group has utilized CDs to decrease the minimum detectable quantity of several drugs [7]. Hurtubise and Richmond [8] have used β-CD/NaCl mixtures to enhance solid-surface luminescence and improved quantification of polynuclear aromatic hydrocarbons. Warner and co-workers [9,10] have studied the effects of alcohol cosolvents on the inclusion complexation of CDs with polynuclear aromatic hydrocarbons. From oxygen quenching studies, these authors found that coinclusion of an alcohol molecule leads to highly protected guest molecules. In a more theoretical study, Eftink's group [11] reported on complexation with a series of alicyclic carboxylates. These authors found that as the size of the carboxylate decreased, the enthalpy and entropy terms for the complexation process became less favorable for less tightly fitting complexes. This result illustrates the importance of optimum host–guest contact in these complexes. Similarly, Turro *et al.* emphasized the importance of "snugness of fit" for CDs used in synthetic schemes [12]. Clearly, a substrate larger than the cavity does not form an inclusion complex at all. However, one which is too small will not complex as favorably as a guest with an optimum fit.

Anilinonaphthalene sulfonic acids (ANS; Fig. 1) are a family of substituted naphthalenes that have been used as extrinsic fluorescent probes for studying the

[1] Department of Chemistry, Acheson Hall, State University of New York at Buffalo, Buffalo, New York 14214.
[2] To whom correspondence should be addressed.

1053-0509/91/0300-0031$06.50/0

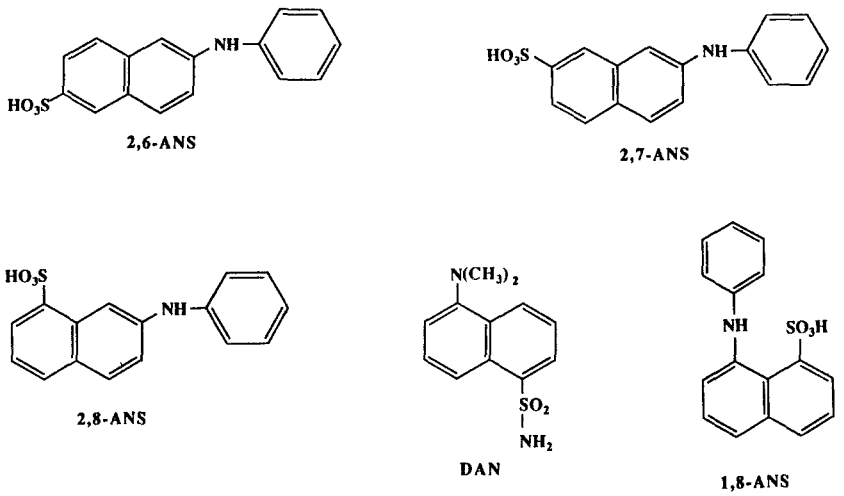

Fig. 1. Structures of the ANS probe molecules used in this study.

structure and dynamics of biochemical domains [13–20] and cyclodextrins [21–27]. They are commonly used because their spectral and temporal characteristics depend on their local microenvironment. Specifically, the substituted naphthalenes we have studied here have low quantum yields and lifetimes in polar media. However, in nonpolar environs, fluorescence and excited-state lifetime can shift dramatically. Thus, these particular probes can be used to report back to us on the local cyclodextrin microenvironment. In addition, if the local environment were to change on a time scale similar to the excited-state lifetime, we could expect these same probes to report on such changes.

Previously, we employed steady-state fluorescence intensities and anisotropies to elucidate (i) the effect of slight changes in ANS structure and (ii) the extent of probe ionization on ANS–β-CD thermodynamics (ΔG, ΔH, and ΔS) [28]. Recently, we extended this work by using multifrequency phase and modulation fluorescence to investigate the decay kinetics of these complexes [29]. We reported [29] that at high β-CD concentrations, in contrast to many earlier reports, these ANS–β-CD inclusion complexes are not described accurately by a small series of discrete decay times. Instead we found that the fluorescence decay kinetics are best described by unimodal continuous lifetime distributions. At that time, however, we were unable actually to determine the best distribution model.

In the present study, we now extend our previous work and aim to determine the most suitable distribution model. Here we have performed a series of new experiments over a range of β-CD concentrations. Again, we use multifrequency phase and modulation fluorescence [30–33] to probe the decay kinetics of five substituted naphthalenes (four ANS derivatives and dansylamide) inclusion complexed with β-cyclodextrin. In a similar fashion to our steady-state studies [28], we now use β-CD titrations as a means to investigate more accurately the dynamical aspects of the ANS–β-CD inclusion complexes. To this end, we employ global analysis techniques [34–39] and fit simultaneously several multifrequency data sets across the entire β-CD titration and search parameter space to yield a self-consistent set of kinetic parameters (i.e., lifetimes and distribution widths).

In all these studies we found that a two-component model was needed to describe the fluorescence decay kinetics. One of the components (the shorter-lived one) was discrete and correlated well with the lifetime for the free (unassociated) probe. The second, longer-lived decay was always best described by a Lorentzian lifetime distribution and the width term was found to decrease with decreasing β-cyclodextrin. This distributed decay process was due to the ANS–β-CD inclusion complex and is of a static nature. That is, dipolar relaxation of the excited-state ANS was not evidenced by our experimental data. Instead we propose, in fact, that we are observing not an excited-state process, but an ensemble [29] of ANS–β-CD complexes in various stages of formation (i.e., ground-state heterogeneity).

EXPERIMENTAL

All fluorescence lifetime measurements were performed with an SLM 48000 MHF multifrequency cross-

correlation phase and modulation fluorometer. For all experiments reported here, the repetition rate of the Pockels cell modulator was 5 MHz. Twenty-five frequencies, at 5-MHz intervals, between 5 and 125 MHz were used to interrogate each sample. Excitation was from the 363.8-nm line of a cw argon-ion laser (Coherent Model 90-6), and emission was monitored through a 420-nm long-pass filter (Oriel). Similar types of conclusions have been drawn using multiwavelength experiments, and here we report on our observation of the "total" fluorescence only. An emission polarizer, oriented at 55° to the vertical was used to eliminate any polarization bias and at least 10 sets of measurements were performed for each sample. In all cases, the experimental data did not vary significantly from set to set. To ensure that there was no sample decomposition, the excitation laser flux (at the sample) was kept below 1 mW. Me_2POPOP (1,4-bis-[4-methyl-5-phenyl-2-oxazolyl]benzene) and POPOP [1,4-bis(5-phenyloxazol-2-yl)benzene], in ethanol, were used as the reference lifetime standards. The arguments and motivation for using multiple-reference fluorophores have been discussed elsewhere [40]. The lifetimes for Me_2POPOP and POPOP were assigned values of 1.45 and 1.31 ns, respectively. In all cases studied, the multifrequency traces recovered using each reference independently were identical and we rule out any systematic deviations within the particular data sets [40]. The sample chamber was thermostated to 25 ± 0.1°C with a Lauda RL6 temperature circulator.

All solutions were prepared in distilled-deionized water and used within 2 weeks of preparation. Stock solutions of β-CD (Astec) were prepared fresh daily. Dansylamide was obtained from Aldrich and 2-anilinonaphthalene-6-sulfonic acid (2,6-ANS), 2-anilinonaphthalene-7-sulfonic acid (2,7-ANS), 2-anilinonaphthalene-8-sulfonic acid (2,8-ANS), and 1-anilinonaphthalene-8-sulfonic acid (1,8-ANS) were obtained from Molecular Probes. Although technically not an ANS derivative, we studied dansylamide because of its structural similarity (Fig. 1). All reagents were used as received after the purity of 10^{-3} *M* stock solutions of each probe was verified by HPLC using a Hibar column (250 mm long × 4 mm in diameter) prepacked with 10 μm LiChrosorb RP-18 (Alltech Associates, Inc.). Absorbance was monitored at 364 nm. Mobile phases of 86:14% (v:v) CH_3CN:H_2O; 50:50% (v:v) CH_3OH:H_2O; and 10:90% (v:v) CH_3CO_2H:H_2O were used, and in all cases greater than 98% of the absorbance was found in a single peak of the chromatogram.

Samples were made by varying β-CD concentrations (10, 6.67, 3.33, 1.67, 0.33, 0.17 m*M*) at a fixed fluorophore concentration of 10^{-5} *M*. At this concentration level, all solutions were free of primary and secondary interfilter effects [28]. Lifetime data for each β-CD titration were analyzed using a global, simultaneous analysis algorithm described by Beechem and Gratton [39]. In all cases the global analysis files contained 300 data points [6 samples × (25 phase angles + 25 demodulation factors)].

THEORY

The basis of phase and modulation fluorescence spectroscopy has been reviewed in detail elsewhere [30–33]. We apply this technique to a series of ANS–β-CD solutions which vary only in the concentration of β-CD.

Traditionally, the fluorescence intensity decay [$I(t)$] is described by a sum of (n) discrete exponentials of the form

$$I(t) = \sum (f_i/\tau_i)\exp(-t/\tau_i) = \sum \alpha_i \exp(-t/\tau_i) \quad (1)$$

Here α_i and f_i are the preexponential (amplitude) factors and fractional intensity contributions to the total fluorescence, respectively, corresponding to lifetime τ_i. The fractional intensity of the ith component to the total fluorescence is given by

$$f_i = \alpha_i\tau_i / \sum \alpha_i\tau_i \quad (2)$$

where $\Sigma f_i = 1$.

Recent reports [29,41–56] have shown that systems originally described by discrete decay processes [Eq. (1)] are more accurately described as continuous distributions of decay times. Using this approach, the fluorescence intensity decay can be written as

$$I(t) = \int [f(\tau)/\tau] \exp(-t/\tau)\, d\tau = \int \alpha(\tau)\exp(-t/\tau)\, d\tau \quad (3)$$

In the present work, uniform (U), Gaussian (G), and Lorentzian (L) continuous lifetime distributions are used to describe $f(\tau)$

$$f_U(\tau) = A \quad \text{from } \langle\tau\rangle - (W/2) \text{ to } \langle\tau\rangle + (W/2) \quad (4a)$$

$$f_U(\tau) = 0 \quad \text{beyond this range} \quad (4b)$$

$$f_G(\tau) = \{A/\sqrt{2\pi\sigma}\}\{\exp[-(\tau - \langle\tau\rangle)^2/2\sigma^2] \quad (5)$$

$$f_L(\tau) = A/\{1 + [(\tau - \langle\tau\rangle)/(W/2)]^2\} \quad (6)$$

where A is constant from the normalization condition: $\int f(\tau) = 1$, $\langle\tau\rangle$ is the mean (center) value of the lifetime distribution, W is the full width at half-maximum (FWHM)

for the uniform and Lorentzian functions, and σ is the standard deviation for the Gaussian.

The multifrequency fluorescence data are fit as described elsewhere [30–33] by minimization of the χ^2 function.

All results reported here are in terms of $\alpha(\tau)$ directly.

RESULTS AND DISCUSSION

The ANS probes chosen for this work exhibited formation constants (K_f) that range from a low of 60 M^{-1} to a high of over 2000 M^{-1} [28]. Thus, based solely on the structure of the probe we could hope to explore the effects of complex strength on the fluorescence decay kinetics.

Figure 2 shows an abbreviated multifrequency data set for the 2,6-ANS–β-CD system. The open and filled symbols represent phase angle and demodulation factor measurements, respectively. In a typical experiment, six data files are analyzed simultaneously; only three are shown here for clarity. The 2,6-ANS-β-CD system is an interesting case study because we found it to be the most difficult to analyze. That is, based upon χ^2 alone, it was difficult to choose one model over another similar model. As a result, this system represents our worst-case scenario, but we stress that we are ultimately able to arrive at a reasonable model for this and all the other ANS-β-CD systems (see below).

Table I compiles the results of global analysis fits to the 2,6-ANS–β-CD data. Clearly, the single expo-

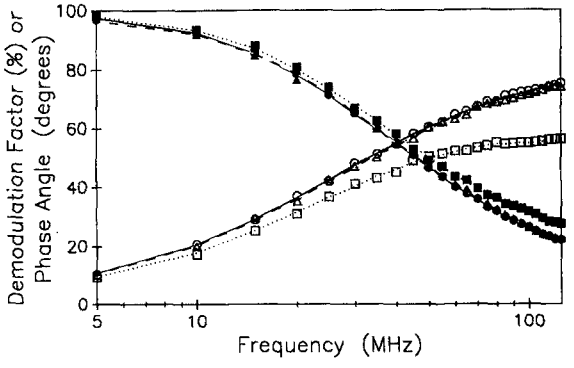

Fig. 2. Phase-modulation plots for 2,6-ANS–β-CD system. (○, ●) 10 mM, (△, ▲) 3.33 mM, and (□, ■) 0.33 mM β-CD. Filled symbols represent the demodulation factor and open symbols denote the phase angle. The lines through the data are the best discrete-distributed Lorentzian fits to the experimental data. Table I compiles the recovered decay parameters.

Table I. Recovered Decay Times for the Global Analysis of 2,6-ANS–β-CD[a]

T_1	T_2	T_3	w_1	w_2	a_1	a_2	χ^2
5.48	—	—	—	—	1.000	—	496
0.54	6.05	—	—	—	0.162	—	4.36
					0.169		
					0.197		
					0.250		
					0.495		
					0.638		
0.40	5.66	14.2	—	—	0.153	0.815	1.25
					0.155	0.798	
					0.186	0.780	
					0.245	0.733	
					0.527	0.460	
					0.669	0.324	
3.81 (G)	—	—	3.84	—	1.000	—	134
			3.78				
			3.76				
			3.63				
			3.22				
			2.73				
4.35 (L)	—	—	2.85	—	1.000	—	290
			2.79				
			2.78				
			2.64				
			2.29				
			1.82				
1.01 (U)	—	—	9.01	—	1.000	—	174
			8.92				
			8.86				
			8.62				
			7.67				
			6.67				
0.42	5.68 (G)	—	—	1.50	0.100	—	1.36
				1.36	0.115		
				1.42	0.149		
				1.12	0.229		
				1.13	0.513		
				0.87	0.663		
0.38	5.74 (L)	—	—	1.19	0.087	—	
				1.10	0.099		
				1.13	0.109		
				0.94	0.193		
				0.93	0.496		
				0.75	0.648		
0.49	5.92 (U)	—	—	5.22	0.191	—	9.50
				5.08	0.221		
				4.25	0.335		
				3.21	0.492		
				1.76	0.662		
				0.99	0.787		
0.41	5.84 (G)	—	—	1.27	0.084	—	1.86
					0.109		
					0.137		
					0.224		
					0.525		
					0.656		

Table I. Continued

T_1	T_2	T_3	w_1	w_2	a_1	a_2	χ^2
0.38	5.73 (L)	—	—	0.97	0.085	—	1.64
					0.096		
					0.109		
					0.202		
					0.494		
					0.637		
0.44	6.03 (U)	—	—	3.98	0.222	—	14.6
					0.295		
					0.391		
					0.544		
					0.628		
					0.854		
0.33 (G)	5.83 (G)	—	0.00	1.58	0.094	—	1.68
			0.00	1.43	0.128		
			0.19	1.44	0.186		
			0.20	1.13	0.286		
			0.14	1.23	0.562		
			0.15	1.01	0.706		
0.32 (L)	5.72 (L)	—	0.00	1.21	0.096	—	1.03
			0.00	1.12	0.126		
			0.26	1.18	0.195		
			0.00	0.96	0.279		
			0.07	0.94	0.559		
			0.14	0.84	0.702		
0.24 (U)	5.86 (U)		0.00	2.54	0.098	—	3.04
			0.04	2.32	0.092		
			0.19	2.43	0.079		
			0.29	1.89	0.870		
			0.33	1.87	0.092		
			0.23	1.57	0.092		

[a] The six entries for the majority of the a_1 and a_2 terms represent (in descending order) 10, 6.67, 3.33, 1.67, 0.33, and 0.17 m*M* β-CD. T_1, T_2, and T_3: recovered discrete or central fluorescence lifetimes (ns). w_1 and w_2: full width at half-maximum for the uniform and Lorentzian and standard deviation for the Gaussian distribution (ns). a_1 and a_2: preexponential factors.

nential decay model can be eliminated (χ^2 = 496) as a accurate description of the true decay kinetics. Similarly, we reject the globally analyzed double (χ^2 = 4.36; 8 floating parameters) and triple (χ^2 = 1.25; 15 floating parameters) exponential decay laws. In addition, we eliminate all unimodal decay models (χ^2 > 130). Of the remaining simple decay models tested, the discrete plus a Lorentzian distribution (χ^2 = 1.04; 14 floating parameters) is chosen over the bimodal Lorentzian decay (χ^2 = 1.03; 20 floating parameters) for two reasons. First, for the bimodal Lorentzian fit, the FWHM for the shorter component varies wildly throughout the titration (Table I). Second, the difference in χ^2 (0.01 unit) is completely insignificant even considering the large degrees of freedom used in this work [57]. Moreover, such a small improvement in χ^2 is certainly not evidence enough to choose a model containing six additional floating parameters. From all these results, we conclude that the best-fit model is a discrete component plus a Lorentzian distribution.

We investigated this system in further detail (Table I) to determine if the FWHM or center lifetimes depended on the concentration of β-CD. We found that floating simultaneously all the center lifetime values and the FWHM resulted in a χ^2 value that was 1.35-fold poorer than when the center lifetime value was linked throughout the analysis (results not shown). Further, when allowed to float, the recovered center lifetimes were randomly fluctuating and were within ±5% of the value when it was linked throughout the global analysis. We thus concluded that the central value of the lifetime distribution was not affected by the concentration of β-CD. In contrast, a similar investigation of the FWHM showed clearly (χ^2 = 1.04 vs 1.64) that it was necessary to allow the FWHM to float independently of one another throughout the analysis in order to achieve a reasonable fit. By doing this, we found that there was a clear trend and the FWHM increased with increasing β-CD (Fig. 3).

In general, all ANS–β-CD systems investigated were best fit by this same type of decay model, i.e., a two-component decay law with a short, discrete and a long, distributed component. The distribution width was found to decrease with decreasing β-CD (Fig. 3), but the center values for each particular ANS probe were unaffected by the β-CD concentration. For the remainder of this discussion we refer to this as the discrete-distributed model. The discrete component was always within 6% of the lifetime for the free probe recovered from separate

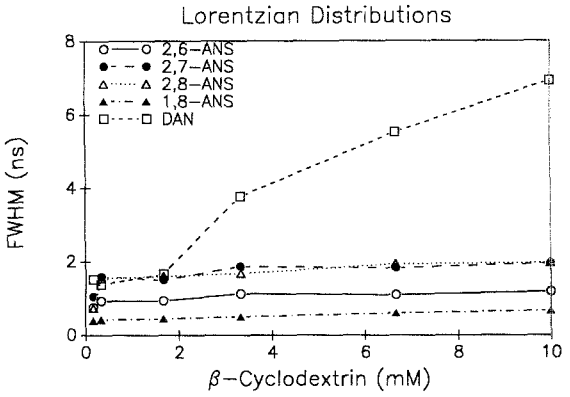

Fig. 3. Recovered Lorentzian FWHM vs β-CD for the various probes used in this study.

experiments. In addition, we found that fixing this lifetime to its "true" value did not alter the recovered decay parameters or the χ^2 value appreciably. The discrete-distributed (Lorentzian) results for the remaining ANS probes are collected in Table II.

The next issue we were concerned with was the uncertainty (precision) in the recovered parameters. To investigate this we performed confidence interval analysis on each parameter. In this approach, we interrogate sequentially the χ^2 surface for each parameter by fixing it and floating all remaining fit parameters. The χ^2 is again minimized by adjusting simultaneously the remaining unfixed fit parameters. Once this new χ^2 minimum is so determined, the parameter of interest is stepped on to its next value and held constant and χ^2 is again minimized. This process is repeated until all the terms of interest have been analyzed over broad enough regions of parameter space.

Figure 4 illustrates the χ^2 surfaces for the discrete and distributed lifetime component of the 2,6-ANS–β-CD system. The pair of horizontal dashed lines represent the one- and two-standard deviation cutoffs for these parameters. From these results, we estimate (at the one-standard deviation level) that the recovered parameters are 0.38 ± 0.06 and 5.74 ± 0.12 ns for the discrete and distributed decay times, respectively. Again, compared to the other probes studied, this represents the worst case results.

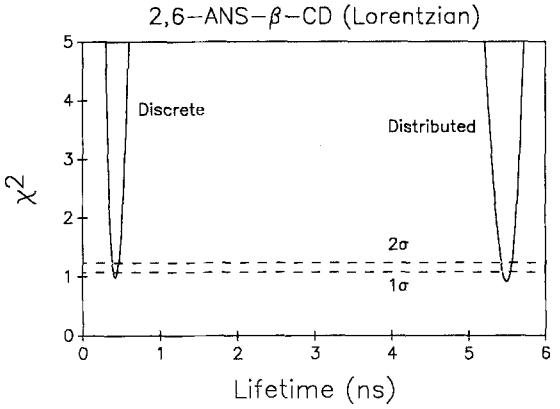

Fig. 4. Recovered χ^2 confidence interval surfaces for the discrete and distributed components of the 2,6-ANS–β-CD inclusion complex.

Table II. Recovered Discrete-Distributed (Lorentzian) Decay Parameters for the Probe–β-CD Inclusion Complexes[a]

Probe	T_1	T_2	w_2	a_1	χ^2
2,7-ANS	1.16	9.26	1.96	0.100	0.96
			1.83	0.139	
			1.87	0.179	
			1.51	0.266	
			1.59	0.611	
			1.05	0.756	
2,8-ANS	0.42	6.35	1.97	0.233	1.05
			1.94	0.313	
			1.68	0.459	
			1.61	0.661	
			1.54	0.892	
			0.73	0.938	
1,8-ANS	0.32	2.03	0.67	0.336	1.10
			0.60	0.391	
			0.50	0.574	
			0.45	0.696	
			0.42	0.892	
			0.39	0.951	
Dansylamide	2.76	9.79	6.93	0.369	0.95
			5.53	0.521	
			3.78	0.722	
			1.67	0.844	
			1.38	0.940	
			1.52	0.966	

[a] The six entries for all the a_1 terms represent (in descending order) 10, 6.67, 3.33, 1.67, 0.33, and 0.17 m*M* β-CD. T_1 and T_2: recovered fluorescence lifetimes (ns). w_2: full-width at half-maximum for the distribution (ns). a_1: preexponential factor for the discrete component.

Figures 5A–F shows the recovered amplitude distributions [$\alpha(\tau)$ vs τ] for the 2,6-ANS–β-CD system as a function of β-CD (A, 10; B, 6.67; C, 3.33; D, 1.67; E, 0.33; F, 0.17 m*M*). A few trends are worth noting. First, the mole fraction of the short decay component increases with decreasing β-CD. This is consistent with a simple equilibrium of the form

$$\underset{\text{(discrete)}}{\text{ANS}} + \text{β-CD} = \underset{\text{(distributed)}}{\text{ANS-β-CD}} \qquad (7)$$

where the uncomplexed ANS corresponds to a short, discrete decay time (similar to ANS free in solution) and the distributed decay time is associated with the bound 2,6-ANS. The second trend (Table I) that is observed, albeit not completely obvious from Fig. 5, is the decrease in half-width with decreasing β-CD (Fig. 3). This result is consistent with the ANS probe sampling fewer and fewer total unique environments as the β-CD concentration is decreased.

Figure 6 shows a plot of the average relative distribution width (FWHM/$\langle\tau\rangle$) for each probe as a function of complex formation constant (K_f). The relative width was chosen to minimize affects due to the difference in the actual decay times of each probe. Clearly, as the formation constant increases (i.e., complexation

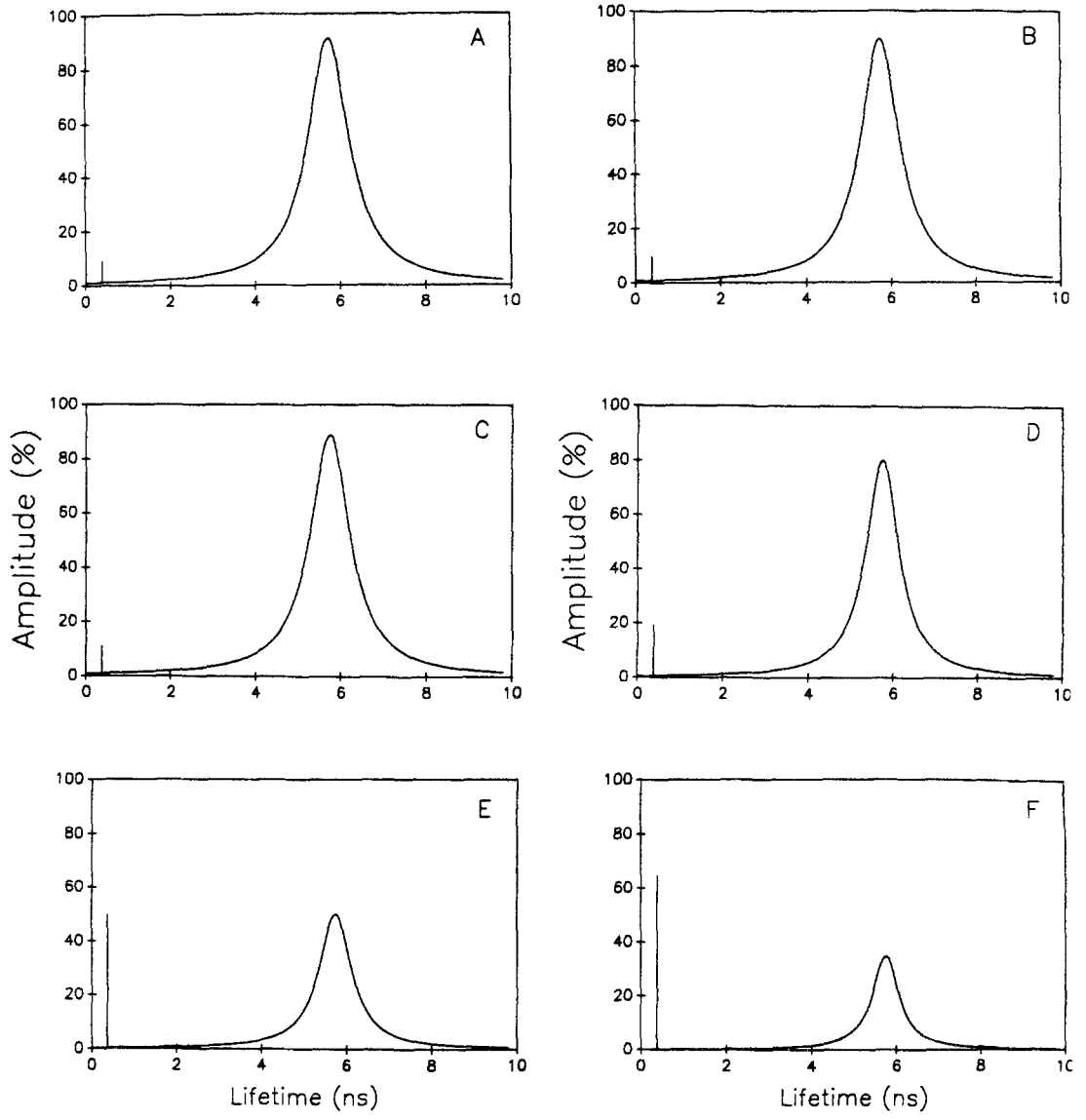

Fig. 5. Complete discrete-distributed amplitude distribution traces for the 2,6-ANS–β-CD system. A, 10 m*M* β-CD; B, 6.67 m*M* β-CD; C, 3.33 m*M* β-CD; D, 1.67 m*M* β-CD; E, 0.33 m*M* β-CD; F, 0.17 m*M* β-CD.

strengthens), the relative width decreases. This result is consistent with the stronger complexes probing fewer, less unique environments, compared to the less strongly complexed probes (e.g., dansylamide). That is, a probe that is less strongly complexed by β-CD is exposed to significantly more relative environmental heterogeneity.

Clearly, there is some form of polarity (environmental) gradient between an ANS probe being completely buried within the β-CD cavity and its being free in aqueous solution. However, such a gradient is certainly not linear. In fact, one would assume that the greatest-disparity, largest gradient occurs at the interface of the cyclodextrin cavity and the nearest-neighbor water molecules. Similarly, one would expect the smallest gradients to occur in bulk solution and at the center of the cyclodextrin cavity.

Thus, if we consider the 2,6-ANS–β-CD case, one would expect several things. First, because of its geometry (Fig. 1) and from CPK models, we would expect 2,6-ANS to complex most effectively with the β-CD. This is in fact the case [28]. Similarly, we would expect this probe to locate deep within the cyclodextrin cavity

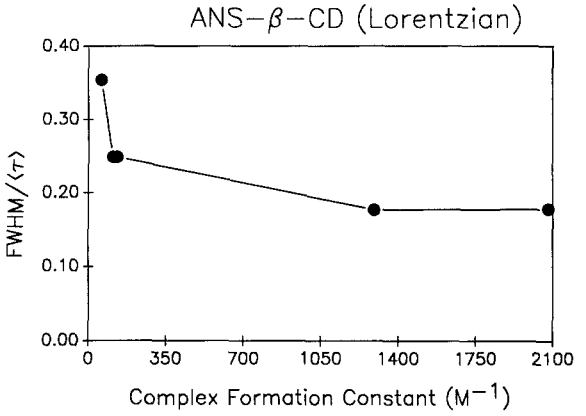

Fig. 6. Average relative distribution width (FWHM/⟨τ⟩) vs probe–β-CD formation constant.

to enhance favorable interactions. Of course, the probe could move within this cavity. However, because the gradient within the cavity is small and the complex is strongly held together, such movement on average would not expose a significant population of 2,6-ANS to a hydrophilic environment. Therefore, while a distribution might be expected and is, in fact, observed (Fig. 5), it certainly would not be extremely broad (on a relative scale).

If we now look to the dansylamide case, we find (compared to 2,6-ANS) that it cannot complex deeply within the β-CD cavity. CPK models show clearly that the naphthalene moiety does not fit too far into the β-CD cavity, and as expected the formation constant is quite small [28]. The dansylamide–β-CD complex is formed more at (compared to 2,6-ANS) the periphery of the cyclodextrin cavity. Like the 2,6-ANS it, too, can move within or from this location. However, because the complex is far weaker, it can dissociate (recall $K_f = k_{in}/k_{out}$) more rapidly. Moreover, since the dansylamide is located much nearer to the "high" gradient region, one would expect a significantly broader distribution. Again, compared to 2,6-ANS we see (Table II; Fig. 3) that dansylamide exhibits a relative distribution width that is about 80% broader.

As expected, the other probes with intermediate K_f and varying geometries exhibit intermediate relative distribution widths (Fig. 6). This reflects both the particular ANS–β-CD environment of complexation (how deep the ANS buries within the cyclodextrin cavity) and the strength of the complex.

CONCLUSIONS

Multifrequency phase and modulation fluorescence in concert with a global data analysis scheme allows us to investigate the detailed dynamics of substituted naphthalenes inclusion complexed with β-cyclodextrin. Our results show that (i) the fluorescence intensity decay is most accurately described by a discrete-distributed decay model, (ii) the distribution is of Lorentzian form, (iii) the center values are independent of the cyclodextrin concentration, (iv) the distribution width is cyclodextrin dependent, (v) the relative distribution width depends on the specific probe used, and (vi) the continuous distribution is a result of an ensemble of ANS–β-CD complexes in the ground state. Item v is the result of the probe "seeing" fewer and fewer unique environments as the cyclodextrin concentration is decreased. The final item (No. vi) is the result of two cooperative processes. The first is the strength of the complex (i.e., K_f). The second is the geometry (structure) of the probe, which serves to locate it on average in regions of high (water–cyclodextrin interface) or low (interior of the cyclodextrin cavity) environmental heterogeneity.

ACKNOWLEDGMENTS

This work was generously supported, in part, by a Non-Tenured Faculty Grant from 3M, Inc., the Health-Care Instruments and Devices Institute at SUNY—Buffalo, and the National Science Foundation (CHE-8921517).

REFERENCES

1. W. Saenger (1980) *Angew. Chem. Int. Ed. Engl.* **19**, 344–360.
2. M. L. Bender and M. Komiyama (1978) *Cyclodextrin Chemistry*, Springer-Verlag, Berlin.
3. R. Breslow (1982) *Science* **218**, 532–537.
4. G. Weber, H. G. Drickamer, and P. M. Torgerson (1979) *Biochemistry* **18**, 3079–3083.
5. D. W. Armstrong, A. Alak, K. Bui, W. Demond, T. Ward, and T. E. Riehl (1984) *J. Incl. Phenom.* **2**(3-4), 533–545.
6. D. W. Armstrong and W. Li (1990) *Anal. Chem.* **62**, 214–217.
7. L. J. Cline-Love, M. L. Grayeski, J. Noroski, and R. Weinberger (1985) *Anal. Chim. Acta* **170**, 3–12.
8. R. J. Hurtubise and M. D. Richmond (1989) *Anal. Chem.* **61**, 2643–2647.
9. I. M. Warner, G. Patonay, and G. Nelson (1988) *Anal. Chem.* **60**, 274–279.
10. G. Nelson, S. Neal, and I. M. Warner (1988) *Spectroscopy* **3**(8), 24–28.
11. M. R. Eftink, M. L. Andy, K. Bystrom, H. D. Perlmutter, and D. S. Kristol (1989) *J. Am. Chem. Soc.* **111**, 6765–6772.
12. N. J. Turro, N. Han, and V. P. Rao (1990) *Tetrahedron Lett.* **31**(6), 835–838.
13. D. M. Worah, K. M. Gibboney, S. S. Yang, and S. S. York (1978) *Biochemistry* **17**, 4487–4492.
14. E. M. Kosower and H. J. Dudiuk (1978) *J. Phys. Chem.* **82**, 2012–2015.

15. D. M. Mock, G. Langford, D. Dubois, N. Criscimagna, and P. Horowitz (1985) *Anal. Biochem.* **151**, 178–181.
16. L. Brand and J. R. Gohlke (1972) *Annu. Rev. Biochem.* **41**, 843–868.
17. C. J. Seliskar and L. Brand (1971) *J. Am. Chem. Soc.* **93**, 5405–5413.
18. C. −H. Huang and J. P. Charlton (1972) *Biochemistry* **11**, 735–740.
19. K. H. Grellman and U. Schmitt (1982) *J. Am. Chem. Soc.* **104**, 6267–6272.
20. D. J. Jobe, R. E. Verrall, R. Palepu, and V. C. Reinsborough (1988) *J. Phys. Chem.* **92**, 3582–3586.
21. C. J. Seliskar and L. Brand (1971) *Science* **171**, 799–800.
22. F. Cramer, W. Saenger, and H.-Ch. Spatz (1967) *J. Am. Chem. Soc.* **89**, 14–20.
23. T. Kinoshita, F. Iinuma, and A. Tsuji (1974) *Chem. Pharm. Bull.* **22**, 2735–2738.
24. H. Kondo, H. Nakatani, and K. Hiromi (1976) *Carbohyd. Res.* **52**, 1–10.
25. J. W. Park and H. J. Song (1989) *J. Phys. Chem.* **93**, 6454–6458.
26. A. Harada, M. Furue, and S. I. Nozakura (1980) *Polymer J.* **12**, 29–33.
27. V. Crescenzi, A. Gamini, A. Palleschi, and R. Rizzo (1986) *Gazz. Chim. Ital.* **116**, 435–440.
28. G. C. Catena and F. V. Bright (1989) *Anal. Chem.* **61**, 905–909.
29. F. V. Bright, G. C. Catena, and J. Huang (1990) *J. Am. Chem. Soc.* **112**, 1343–1346.
30. D. M. Jameson, E. Gratton, and R. D. Hall (1984) *Appl. Spectrosc. Rev.* **20**, 55–106.
31. J. R. Lakowicz, G. Laczko, I. Gryczynski, H. Szmacinski, and W. Wiczk (1988) *J. Photochem. Photobiol. B Biol.* **2**, 295–311.
32. E. Gratton, D. M. Jameson, and R. D. Hall (1984) *Annu. Rev. Biophys. Bioeng.* **13**, 105–124.
33. F. V. Bright, T. A. Betts, and K. S. Litwiler (1990) *CRC Crit. Rev. Anal. Chem.* **21**, 389–405.
34. J. R. Knutson, J. M. Beechem, and L. Brand (1983) *Chem. Phys. Lett.* **102**, 501–507.
35. J. M. Beechem, J. R. Knutson, J. B. A. Ross, B. W. Turner, and L. Brand (1983) *Biochemistry* **22**, 6054–6058.
36. J. M. Beechem, M. Ameloot, and L. Brand (1985) *Chem. Phys. Lett.* **120**, 466–472.
37. J. M. Beechem, M. Ameloot, and L. Brand (1985) *Anal. Instrum.* **14**, 379–402.
38. J. M. Beechem and L. Brand (1986) *Photochem. Photobiol.* **44**, 323–329.
39. J. M. Beechem and E. Gratton (1989) *Proc. SPIE* **909**, 70–81.
40. K. S. Litwiler, J. Huang, and F. V. Bright (1990) *Anal. Chem.* **62**, 471–476.
41. W. R. Ware, D. R. James, Y. S. Liu, A. Siemiarczuk, and B. D. Wagner (1988) *Proc. SPIE* **909**, 90–96.
42. J. R. Alcala, E. Gratton, and F. G. Prendergast (1987) *Biophys. J.* **51**, 925–936.
43. J. R. Alcala, E. Gratton, and F. G. Prendergast (1987) *Biophys. J.* **51**, 597–604.
44. J. R. Alcala, E. Gratton, and F. G. Prendergast (1987) *Biophys. J.* **51**, 587–596.
45. A. Siemiarczuk and W. R. Ware (1989) *J. Phys. Chem.* **93**, 7609–7168.
46. D. R. James, Y.-S. Liu, P. DeMayo, and W. R. Ware (1985) *Chem. Phys. Lett.* **120**, 460–465.
47. D. R. James and W. R. Ware (1985) *Chem. Phys. Lett.* **120**, 455–459.
48. B. D. Wagner and W. R. Ware (1990) *J. Phys. Chem.* **94**, 3489–3494.
49. M. L. Barcellona and E. Gratton (1989) *Biochim. Biophys. Acta* **993**, 174–178.
50. R. Fiorini, M. Valentino, S. Wang, M. Glaser, and E. Gratton (1987) *Biochemistry* **26**, 3864–3870.
51. L. J. Libertini and E. W. Small (1989) *Biophys. Chem.* **34**, 269–282.
52. A. Siemiarczuk, B. D. Wagner, and W. R. Ware (1990) *J. Phys. Chem.* **94**, 1661–1666.
53. D. R. James and W. R. Ware (1986) *Chem. Phys. Lett.* **126**, 7–11.
54. E. Kalb, F. Paitauf, and A. Hermetter (1989) *Biophys. J.* **56**, 1245–1253.
55. D. R. James, J. R. Turnbull, B. D. Wagner, W. R. Ware, and N. O. Petersen (1987) *Biochemistry* **26**, 6272–6277.
56. J. Huang and F.V. Bright (1990) J. Phys. Chem. **94**, 8457–8463.
57. P. R. Bevington (1969) *Data Reduction and Error Analysis for the Physical Sciences*, McGraw–Hill, New York, Chap. 10.